

COBE FIRAS observations of Galactic Lines

D. J. Fixsen^{1,3}, C. L. Bennett², and J. C. Mather²

ABSTRACT

The *COBE* Far InfraRed Absolute Spectrophotometer (FIRAS) observations constitute an unbiased survey over the wavelength range from 100 μm to 1 cm over 99% of the sky. Improved calibration of the FIRAS instrument and the inclusion of all of the FIRAS data allow an improved signal to noise determination of the spectral lines by a factor of ~ 2 over our previous results. The resolution is low (0.45 cm^{-1}) so only the strongest lines are observable. The CO chain from $J = 1 - 0$ to $J = 8 - 7$ is observed towards the Galactic center. The line ratios are roughly consistent with a 40 K excitation temperature. The 157.7 μm C II and 205.3 μm N II lines are observable over most of the sky. The 370.4 μm and 609.1 μm lines of C I, and the 121.9 μm line of N II are observed in the Galactic plane. The line ratios at the Galactic center are consistent with a density of $n_0 \sim 30 \text{ cm}^{-3}$ and a UV flux of $G_0 \approx 15 \mu\text{W m}^{-2} \text{ sr}^{-1}$ (10 Habing units). The 269 μm H₂O line is observed toward the Galactic center in absorption.

Subject headings: ISM: atoms, bubbles, general, molecules — line: identification
Galaxy: general

1. Introduction

An unbiased far infrared survey of the spectral line emission from the Galaxy has been reported from the Cosmic Background Explorer (*COBE*) mission by Wright et al. (1991)

¹Raytheon-STX Corp., Code 685, NASA/GSFC, Greenbelt, MD 20771

²Code 685, Infrared Astrophysics Branch, Goddard Space Flight Center, Greenbelt, MD 20771

³email address fixsen@stars.gsfc.nasa.gov

and Bennett et al. (1994). A new analysis of the FIRAS data provides an improvement of approximately a factor of 2 in signal-to-noise and a more complete map of the sky. This has enabled improved full sky maps of the $157.7 \mu\text{m}$ C II and $205.3 \mu\text{m}$ N II cooling lines and additional detections of CO lines, and the $115.8 \mu\text{m}$ CH line. The $269 \mu\text{m}$ H₂O line was detected in absorption towards the Galactic center.

While the primary purpose of the instrument was to make precise measurements of the cosmic microwave background radiation, the instrument design had many advantages for the study of large scale diffuse emission from our Galaxy. The FIRAS has made absolute measurements of intensity with no beam switching, with a 7° beam, and has observed 99% of the sky. This makes the FIRAS data well-suited for determination of diffuse emission. The FIRAS spectral resolution is low, as discussed below in §3, and no spectral lines are resolved. Despite this, the Galactic rotation can be discerned using the detected FIRAS spectral lines (Fixsen et al. 1996).

The absolute nature of the FIRAS measurements coupled with the nearly full sky coverage allow observation of the overall Galactic energy balance. However care needs to be taken in comparing the results to measurements taken with a small beam or done with beam switching. Since the FIRAS beam is large, even bright small sources can appear insignificant while large diffuse regions that don't even appear in beam switched studies dominate.

The first cosmological results from the *COBE* FIRAS instrument were reported by Mather et al. (1990), and Boggess et al. (1992). More recent results are reported by Bennett et al. (1994), Fixsen et al. (1996, 1997, 1998, 1999), and Dwek et al. (1997). Previous results of the *COBE* FIRAS unbiased far infrared survey of the Milky Way were published by Wright et al. (1991) and Bennett et al. (1994). Bennett's Figure 2 summarizes spectral line detections from *COBE* FIRAS: $157.7 \mu\text{m}$ C II, $370.4 \mu\text{m}$ and $609.1 \mu\text{m}$ C I, J=2-1 through J=5-4 CO, and $121.9 \mu\text{m}$ and $205.3 \mu\text{m}$ N II. Since then, improved data processing algorithms and techniques have allowed for a more detailed examination of the data.

The C II, C I and CO emission lines detected by *COBE* are recognized as the expected cooling lines from PDRs (Hollenbach, Takahashi, & Tielens 1991). The result that the Galactic-averaged PDR properties are described by lower excitation conditions than objects such as Orion is reinforced by the weakness of the $145.5 \mu\text{m}$ O I line.

2. Calibration and Line Fitting

The FIRAS instrument and its calibration were described in detail by Fixsen et al. (1994). Significant improvements were noted by Fixsen et al. (1996). In this paper we use the combined (all detectors and all scan modes), destriped data with higher frequency resolution also denoted “Pass 4” (FIRAS Explanatory Supplement). The improved calibration, destriping, and larger data set reduce the uncertainties to about half of those of Bennett et al. (1994). Data from all of the channels, scan modes, and frequency bands were combined using a weighted average to form a data set with 210 spectral points from 4.4 mm to 104 μm (2.3 to 96.3 cm^{-1}). Some of these data were used by Bennett et al. (1994).

The instrument line response function is described in detail by Bennett et al. (1994). Since the apodization is asymmetric, the resulting line profile is complex. For “Pass 4” we padded the 512 point interferograms with an additional 128 points on the short side to include almost all of the information in the real part of the spectrum with a bin width of 0.45 cm^{-1} .

Continuum and line spectra were fitted to the data as follows. First, a 2.728 K Planck spectrum, $P_\nu(T = 2.728)$ was subtracted from the spectrum at each sky pixel. Then the spectrum at each pixel was fit with 36 parameters. The parameters of the fit (and their corresponding degrees of freedom at each pixel) were: the amplitudes at each assumed line frequency (18), the amplitude of a dP/dT term to remove the cosmic microwave dipole (1), the amplitude of a $\nu^{1.6} * P_\nu(18)$ to remove most of the Galactic dust emission (1), and coefficients of Legendre polynomials for the continuum emission of the dust (16). The fit removes 36 degrees of freedom, leaving 174 degrees of freedom at each of 6063 pixels. The data were weighted by an inverse variance that is dominated by detector noise, but calculation of the uncertainties include other terms. The use of this diagonal matrix weighting is an approximation to the full covariance matrix, which is not perfectly diagonal because of the effects of the apodization and the calibration process. The full covariance matrix was used to compute the uncertainties (Fixsen et al. 1994).

The Galactic plane is unresolved by the 7° FIRAS beam. From DIRBE and other observations it is seen that for ($1 \text{ cm} > \lambda > 100 \mu\text{m}$) the Galactic radiation is concentrated in a band 1° wide. For the Galactic plane we use the FIRAS data before they are binned into pixels. We form bins of 5° Galactic longitude and 1° Galactic latitude centered on the Galactic plane. With the assumption that the observations near the Galactic plane are dominated by the radiation from a region 1° across at the Galactic plane, the spectrum for each bin is given by:

$$S_\nu = \sum_i (W_i B_i S_{i\nu}) / \sum_i (W_i B_i^2), \quad (1)$$

where W_i is the weight of the i^{th} data in the bin, B_i is the beam response to a line source at the Galactic plane and $S_{i\nu}$ is the i^{th} spectrum. The beam response is derived from observations near the moon, which are not otherwise used. The beam response is used to derive B , which is normalized to a 1° wide unit line source. This has two important effects. First we increase the signal to noise ratio in the result as we weight the data in proportion to the signal. Second the amplitude is increased by a factor of ~ 8 over the presentation in Bennett et al. (1994). This is because Bennett et al. give an average over $|b| < 5^\circ$ while we give the result for $|b| < 0.5^\circ$. For $|b| > 10^\circ$ we use the pixels from Fixsen (1996).

For each pixel we perform a simultaneous least squares fit of a continuum spectral baseline plus a series of spectral line profiles centered on the wavelengths of known lines. The result is a set of spectral line intensities for each pixel. We find that while the C II emission (Figure 1, top) follows the continuum closely, and the N II emission (Figure 1, bottom) follows it approximately, the CO and other emissions have distinct distributions.

3. Analysis Results

3.1. The CO Emission

The J=1-0, 6-5, 7-6 and 8-7 CO lines are detected, as well as the CO J=2-1, 3-2, 4-3 and 5-4 transitions noted by Bennett et al. (1994). Figure 3 shows CO emission from the central Galactic region. The 7-6 transition appears but the $370.4 \mu\text{m}$ C I and the $369 \mu\text{m}$ 7-6 CO transitions are too close to be resolved by the FIRAS. Some care must be exercised to interpret Figure 3g. This is probably a mixture of the 7-6 CO transition and the C I emission.

Bally et al. (1988) found that in the Galactic center region the low lying rotational CO lines are optically very thick. So, the line emission should be proportional to $\nu^4 * \exp(-E/kT)$, where the extra factor of ν is because the same velocity dispersion leads to higher bandwidth at higher frequencies. With this model, the full CO spectrum can be reasonably approximated by a 40 K temperature (figure 2a). A simple explanation is a temperature distribution with a peak at 40 K. We use this model to estimate the emission due to CO 7-6 and assign the remaining emission to the $370.4 \mu\text{m}$ C I.

There are small regions exhibiting much higher temperatures (Simpson et al. 1997, Jackson et al. 1996). We see only a hint in these data in the form of the high CO 8-7 transition and the uncertainties do not justify a more complex model for the large area-averaged data. The larger uncertainties at higher frequencies allow only upper limits of 10 and $15 \text{ nW m}^{-2} \text{ sr}^{-1}$ respectively for the CO 9-8 and CO 10-9 lines. These results are

in broad agreement with Paglione et al. (1998) who concluded 80% of the gas is 40 K and below. Since the CO is optically thick significant high temperature regions could be hidden from the FIRAS instrument.

There is also a smaller but significant amount of CO emission in the plane at longitudes $2.5 < |l| < 32.5^\circ$. Again we use the thick optical model of CO to fit to a 22 K spectrum (Figure 2b), estimate the emission due to CO 7-6 and assign the remaining emission to the $370.4 \mu\text{m C I}$. These are used in the table.

Over most of figure 2g the signal to noise is too low to estimate the CO temperature. Instead the CO 7-6 emission is approximated as the average of the CO 8-7, CO 6-5 and CO 5-4 emission. The resulting C I (Figure 5c) shows a similar intensity and structure to the $609.1 \mu\text{m C I}$ emission.

3.2. Water Absorption

The ground state $1_{11} - 0_{00}$ $269 \mu\text{m}$ transition of para- H_2O is detected. The longitude profile of this water transition, shown in Figure 4a, displays an absorption dip towards the Galactic center, as do Bennett et al. (1994). With the improved signal to noise ratio we can now detect this line at the $\sim 5\sigma$ level. The error bars on the line intensity are larger near the Galactic center because of uncertainty in the ability to calibrate and remove the larger continuum emission there. As shown by Bennett et al. (1994) the water absorption should be expected.

In Figure 4c we examine the ratio of the $269 \mu\text{m}$ para- H_2O line to the continuum. The change in the ratio shows that this is a true absorption and not an artifact of the calibration. Beyond the central Galactic region ($40^\circ > l > -90^\circ$) the signal is so small that it is swamped by the noise.

3.3. Emission Lines of O, Si, and CH

As oxygen is the third most abundant element, molecular oxygen might be expected in a wide variety of conditions (Viala & Walmsley 1996). Measuring it would help to unravel the many reactions involving oxygen. Searching for it is difficult because of the oxygen in the atmosphere. The $(3_2 - 1_2)$ transition of O_2 at $705.8 \mu\text{m}$ (Figure 4e) is predicted by Marechal et al.(1997) to be among the strongest O_2 lines. The intensity could be up to $10 \text{ nW m}^{-2} \text{ sr}^{-1}$ for thick clouds. The line was not detected by *COBE* FIRAS, and we place a limit (95% CL) on its intensity towards the Galactic center of $1 \text{ nW m}^{-2} \text{ sr}^{-1}$. There is

1 nW m⁻² sr⁻¹ of O₂ in a ring ($|l| \approx 10$ deg) but this is only a 2.5σ effect and we do not claim a detection, but only an upper limit of 3 nW m⁻² sr⁻¹.

The 145.5 μ m O I (Figure 4f) is detected but it is strongest in the spiral arms rather than the Galactic center. The 115.8 μ m CH (Figure 4h) line has been detected, although the FIRAS noise is high. A weighted average using the 205.3 μ m N II intensity as a template improves the signal/noise ratio to show the detection of the 115.8 μ m CH line at the $\sim 3\sigma$ level. Using the same method, the 129.7 μ m Si I line shows a $\sim 2\sigma$ effect (Figure 4g), but we cannot claim a detection and we place an upper limit (95% CL) of 250 nW m⁻² sr⁻¹ towards the Galactic center. None of these lines are evident out of the Galactic plane.

Liu et al. (1997) made a careful search for CH lines in the planetary nebula NGC 7027. They report detections of the rotational lines ${}^2\Pi_{1/2}(F_2)J = 3/2 - 1/2$ at 149.2 μ m (4.6 nW m⁻² sr⁻¹), the ${}^2\Pi_{1/2}(F_2)J = 5/2 - 3/2$ lines at 180.7 μ m (3.7 nW m⁻² sr⁻¹) and the ${}^2\Pi_{3/2}(F_2)J = 5/2 - 3/2$ lines at 115.8 μ m (2.2 nW m⁻² sr⁻¹). They also report an upper limit of 1 nW m⁻² sr⁻¹ on the ${}^2\Pi_{1/2}(F_2)J = 7/2 - 5/2$ lines at 118.6 μ m. The intensities given here are the mean intensities for the 70 arc second beam of the *ISO* long wavelength spectrometer. Most of the radiation originates from a region ~ 5 arc seconds across (Middlemass 1990), which implies an intensity of 440 nW m⁻² sr⁻¹ for the central region. The intensity we observe towards the Galactic center region (that is the region weighted by the N II) is ~ 70 nW m⁻² sr⁻¹. Liu et al. (1996) observe the 157.7 μ m C II to 115.8 μ m CH ratio to be about 150. The ratio we observe using the same selection for C II as for the CH is about 300. The uncertainties are large so the difference may be insignificant or the mean inner Galaxy may have a higher C II to CH ratio than NGC 7027.

The first excited rotational level of CH has a critical density of $\sim 4 \times 10^6$ cm⁻³ and the next level has a critical density of $\sim 10^8$ cm⁻³ (Phelps & Dalby 1966). Although we do not see the 149.2 μ m lines they are in the wings of the very strong 157.7 μ m C II line and the upper limit would allow the same ratio as observed by Liu et al.(1997). Evidently at least part of the radiation emanates from fairly dense regions.

3.4. C II, C I

The 157.7 μ m C II line is clearly the dominant line in this entire band. Examination of the intensity along the Galactic plane (Figure 5a) shows the peak of the C II line is not in the Galactic center but in the molecular ring at $l = \pm 25^\circ$. Other peaks are evident at $\pm 50^\circ, 80^\circ, 110^\circ$, and 135° , with the inner peaks more evident for $l < 0$ and the outer peaks more evident for $l > 0$, clearly demonstrating the spiral structure of the Galaxy.

The C II to continuum ratio is fairly constant both along the Galactic plane and out of the plane with C II enhancements of a factor of 2 or 3 in the spiral arms (Figure 5c).

The 609.1 μm C I (Figure 5b) is almost entirely confined to the inner Galactic region, with a clear peak at the Galactic center and shoulders out to the molecular ring, unlike the C II which has a dip in the Galactic center.

The 370.4 μm C I line can not be separated from the 269 μm CO 7-6 transition, with the FIRAS resolution. We model the CO 7-6 emission as the average of the CO 8-7, CO 6-5 and CO 5-4 emission. The resulting C I (Figure 5c) shows a similar intensity and structure to the 609.1 μm C I emission.

3.5. N II

The 205.3 μm N II line is strong enough to form a reasonable full sky map from the FIRAS data (Figure 1 bottom). It has a similar structure to the C II (Figure 5e) although it is more strongly concentrated in the Galactic center. The N II/C II ratio plotted as a function of Galactic longitude (Figure 5h) shows a smooth function with a peak at the Galactic center. Rudolph et al. (1997) give an N/S abundance ratio variation as $\propto 10^{-.03R}$, where R is the radius in kpc. They note that the S/O ratio is constant as expected. Assuming the S/C ratio is constant, we derive the dashed line in figure 5h for radiation dominated by the inner edge, or the dotted line for uniform sources.

The 121.9 μm N II line (Figure 5f) has a structure and magnitude similar to the 205.3 μm N II line emission. The higher noise of the FIRAS at this frequency prevents a detailed comparison but to first order it appears that the 121.9 μm N II line emission can be modeled as proportional to the 205.3 μm N II line emission. The mean of the $I(121.9 \mu\text{m N II}) / I(205.3 \mu\text{m N II})$ ratio is 1.1 ± 0.1 suggesting most of the N II radiation originates in low density regions (Rubin 1985).

Table 1: Line Flux at High Galactic Latitude

Line	Galactic Center	Inner Galaxy	Outer Galaxy	High Latitudes
	$ l < 2.5^\circ$	$2.5 < l < 32.5^\circ$	$ l > 32.5^\circ$	$ b > 10^\circ$
CO 1-0	1.6 ± 0.5	0.5 ± 0.3	0.2 ± 0.2	$0 \pm .01$
CO 2-1	6.4 ± 0.3	2.3 ± 0.2	0.5 ± 0.1	$0 \pm .01$
CO 3-2	11.8 ± 0.5	3.8 ± 0.3	0.7 ± 0.2	$0 \pm .01$
CO 4-3	17.7 ± 0.6	3.4 ± 0.3	0.5 ± 0.3	$0 \pm .01$
CO 5-4	16.5 ± 1.0	2.9 ± 0.6	0.9 ± 0.5	$.01 \pm .01$
CO 6-5	11.5 ± 1.6	0.5 ± 1.0	-0.2 ± 0.7	$0 \pm .01$
CO 7-6 ¹	10 ± 1.5	0.3 ± 1.0	0.1 ± 0.3	$0 \pm .01$
CO 8-7	10.8 ± 1.4	1.8 ± 0.8	0.1 ± 0.5	$.01 \pm .01$
C I 609 μm	11 ± 0.6	5 ± 0.4	1.4 ± 0.3	$.01 \pm .01$
C I 370 μm ¹	11 ± 1.9	7 ± 1.0	1.4 ± 0.5	$0 \pm .01$
C II 158 μm	875 ± 32	1021 ± 17	254 ± 5	$1.48 \pm .07$
N II 205 μm	97 ± 6	107 ± 3	18 ± 1	$.05 \pm .02$
N II 122 μm	76 ± 51	23 ± 22	2 ± 9	$.17 \pm .14$
O I 146 μm	29 ± 29	24 ± 13	5 ± 5	$.07 \pm .08$
CH 116 μm	149 ± 82	14 ± 34	15 ± 15	$-.05 \pm .25$
Dust Emission	130000	92000	25000	150

Units are $\text{nW m}^{-2} \text{sr}^{-1}$. Uncertainties are 1σ and include systematic effects.

¹The CO 7-6 was estimated from the other CO lines and the residual was ascribed to C I.

3.6. Galactic Center

In figures 1, 3, 4, and 5 the Galactic center stands out as a distinct region. Only there is the CO 1-0 detectable. The CO line ratios suggest a temperature of 40 K (Figure 2). We attempt to fit the observed line strengths of CO 1-0 thru CO 8-7, the C I lines and the C II line by adjusting the density, UV flux and an overall gain to the the PDR model of Hollenbach et al. The best fit is $n_0 = 30 \text{ cm}^{-3}$ and $G_0 = 15 \mu\text{W m}^{-2} \text{sr}^{-1}$ (10 Habing units). The fit is only weakly dependent on the density, allowing a factor of 5 in either direction. The data constrain the UV flux much better, allowing only a factor of 2 in G_0 . The fit is poor ($\chi^2/\text{DOF}=58$) with the major problem being the observed C II line intensity which is a factor of 3 higher than the model. This might be due to foreground or background emission from the molecular ring. Thus we can make the model agree with the ratios if we assume

a density of $\sim 30 \text{ cm}^{-3}$ and a UV density of $G_0 = 15 \mu\text{W m}^{-2} \text{ sr}^{-1}$ and that much of the observed C II flux at the Galactic center is really from the molecular ring. The density is in agreement with the Bally et al. (1988) average density estimate of 50 cm^{-3} over the region $r < 500 \text{ pc}$, $|h| < 100 \text{ pc}$, which is approximately the same as our Galactic center region.

The values we obtained for G_0 and n_0 are lower than other observers (Simpson et al. 1997) have found in the Galactic Center. They used much smaller beamwidths and were sensitive to compact objects, while our beamwidth of 7° corresponds to a region 1 kpc across. Our numbers are also small compared to those we found for the inner Galaxy region defined below. We conclude that the high brightness of the Galactic Center is due to relatively low density material filling a relatively large fraction of available space, rather than compact objects around young stars.

3.7. Inner Galaxy

A second distinct region is the inner Galaxy, roughly the Galactic plane with $2.5 < |l| < 32^\circ$. This region has much smaller CO emission even though it has more C I emission. The CO emission is consistent with an optically thick temperature of 22 K, considerably cooler than the Galactic center. Fitting the PDR model to the data yields $n_0 > 5000 \text{ cm}^{-3}$ and $G_0 > 800 \mu\text{W m}^{-2} \text{ sr}^{-1}$. Even so there is a factor of 2 more C II emission observed than the model prediction. This suggests that in the inner Galactic regions the lines emission is from dense clouds with high UV flux, and that the C II emission is more efficient than in the one dimensional PDR model. This could be a simple surface to volume ratio effect.

3.8. Outer Galaxy

The outer Galactic plane presumably should also be similar to local conditions averaged over a sufficiently large volume. This region has approximately the same line ratios as the inner Galaxy suggesting the conditions are much the same on average although the average emission is a factor of 5 lower than the inner Galaxy. The one exception is that the N II to C II ratio is lower. This can be explained by a generally lower N abundance in the outer Galaxy (Rudolph et al.1997).

3.9. High Latitude Emission

The high latitude emission is much weaker than the emission in the outer Galactic plane. The simple picture of a thin disk ($R/t \sim 100$) gives just this effect with the same line ratios as observed in the outer Galaxy. This description holds although the signal/noise ratios for most of the lines are too small to make a strong statement.

4. Conclusions

1. The *COBE* FIRAS has conducted an unbiased survey of the far-infrared emission from our Galaxy. Previous results of this survey were reported by Wright et al. (1991) and Bennett et al. (1994). We report here the distribution along the Galactic plane ($b = 0^\circ$) of the spectral line emission for the detected spectral lines.
2. The CO line ratios suggest an excitation temperature of 40 K in the Galactic center and ~ 20 K in other typical regions of CO emission.
3. We find the PDR model of Hollenbach fits the observed line ratios in the Galactic center if we assume a density of $\sim 30 \text{ cm}^{-3}$ and a UV flux of $G_0 \approx 15 \mu\text{W m}^{-2} \text{ sr}^{-1}$.
4. We find the C II emission observed is higher than the PDR model of Hollenbach over the source regions in the rest of the Galaxy, even if we assume high densities $> 5000 \text{ cm}^{-3}$ and high UV flux $G_0 > 800 \mu\text{W m}^{-2} \text{ sr}^{-1}$ in the emission regions.
5. The $205.3 \mu\text{m}$ line of N II generally follows the $157.7 \mu\text{m}$ C II line distributions, but there is probably an abundance effect that enhances the N II intensity in the inner Galaxy.
6. We have detected the $115.8 \mu\text{m}$ CH line in the inner Galactic region and the $269 \mu\text{m}$ H₂O line in absorption towards the Galactic center.

COBE is supported by NASA's Astrophysics Division. We are grateful for the contributions of the entire *COBE* Science Team and the support personnel at Goddard's Cosmology Data Analysis Center (CDAC). We thank G. Hinshaw for help with plots and pictures.

REFERENCES

- Bally, J. et al. 1988, ApJ, 324, 223
- Bennett, C. L. et al. 1994, ApJ, 434, 587
- Boggess, N. W. et al. 1992, ApJ, 397, 420
- COBE Far Infrared Absolute Spectrophotometer (FIRAS) Explanatory Supplement, 1997, ed. S. Brodd, D. J. Fixsen, K. A. Jensen, J. C. Mather and R. A. Shafer, COBE Ref. Pub. No. 97-C (Greenbelt, MD: NASA/GSFC), available in electronic form from the NSSDC.
- Dwek, E. et al. 1997, ApJ, 475, 565
- Fixsen, D. J. et al. 1994, ApJ, 420, 457
- Fixsen, D. J. et al. 1996, ApJ, 473, 576
- Fixsen, D. J. et al. 1997, ApJ, 486, 623
- Fixsen, D. J. et al. 1998, ApJ, 508, 123
- Fixsen, D. J. et al. 1999, ApJ, 512, TBD
- Hollenbach, D., Takahashi, T. & Tielens, A.G.G.M. 1991, ApJ, 377, 192
- Jackson, J. M. et al. 1996, ApJ, 456, L91
- Liu, X. W. et al. 1996, A&A, 315, L257
- Liu, X. W. et al. 1997, Mon.Not.R.A.S., 290 L71
- Marechal, P. et al. 1997, A&A, 324 221
- Mather, J. C. et al. 1990, ApJ, 354, L37
- Mather, J. C. et al. 1994, ApJ, 420, 439
- Middlemass, D. 1990, Mon.Not.R.A.S., 244, 294
- Paglione, T. A. D. et al. 1998, ApJ, 324, 680
- Phelps, D. H., Dalby, F. W., 1966 Phys. Rev. Lett., 16, 3
- Reynolds, R. J. 1992, ApJ, 392, L35
- Reynolds, R. J. 1990, The Galactic and Extragalactic Background Radiation, S. Bowyer & C. Leinert eds., p157
- Rudolph, A. L. et al. 1997, ApJ, 489, 94
- Simpson et al. 1997, ApJ, 487, 689
- Viala, Y. P. & Walmsley, C. M. 1976, A&A, 50, 1

Wright, E. L. et al. 1991, ApJ, 381, 200

FIGURE CAPTIONS

Figure 1:(Color Plate) The maps are projections of the full sky in Galactic coordinates. The plane of the Milky Way is horizontal in the middle of the map with the Galactic center at the center. Galactic longitude $l = 90^\circ$ is left of center. The maps are smoothed to 10° resolution. The black stripes are unobserved portions of sky. Color bars indicate emission intensity in $\text{nW m}^{-2} \text{sr}^{-1}$. The scale is not linear. (*top*): A full sky map of $157.7 \mu\text{m}$ C II emission from the *COBE* FIRAS experiment. (*bottom*): A full sky map of $205.3 \mu\text{m}$ N II emission from the *COBE* FIRAS experiment.

Figure 2:The spectrum of the CO chain at the Galactic center. The solid line is a 40 K fit. The dotted lines are 35 K and 45 K. The CO 7-6 point was not used in the fit. The error bars are 1σ . The lower plot is the inner Galactic region with a fit of 22 K.

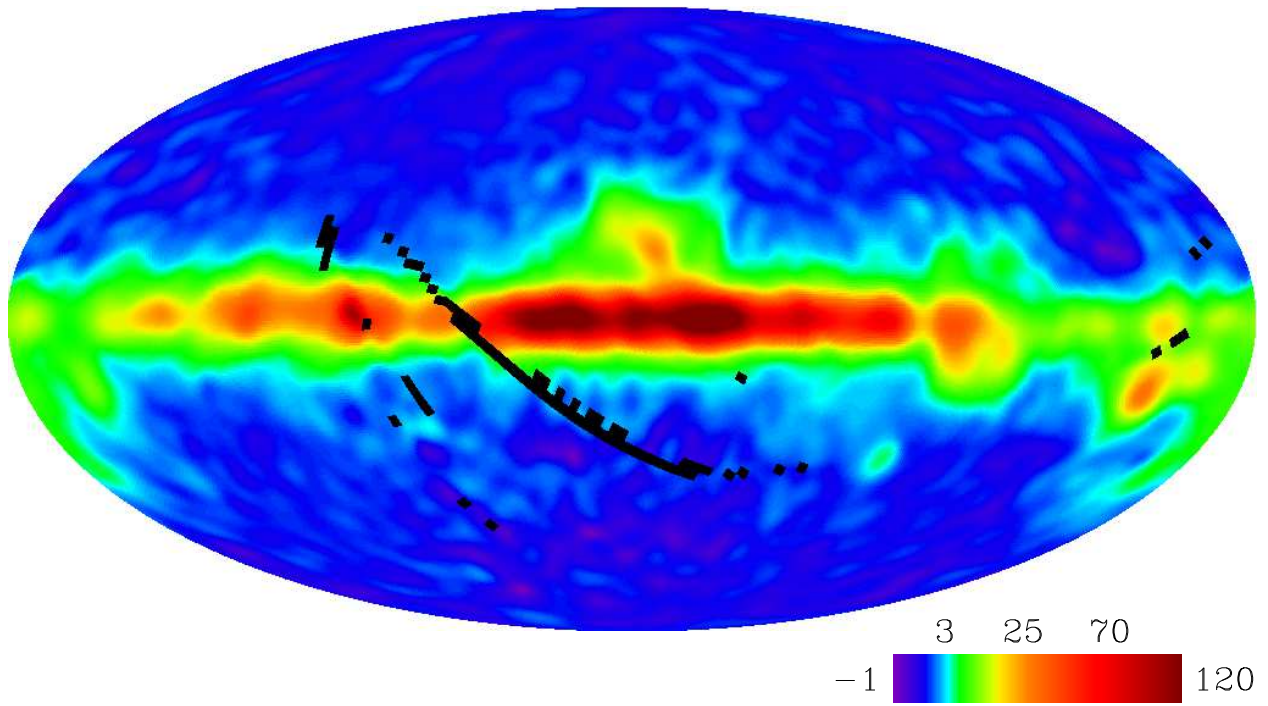
Figure 3: Longitude profiles of the intensity for CO lines for the Galactic plane. The intensity in each bin represents the average over 5° in Galactic longitude and $\pm 0.5^\circ$ in Galactic latitude, under the assumption that the emission is dominated by an unresolved line at the Galactic plane. The 2σ error bars include detector noise and gain uncertainties. There are few measurements in the $l = 90^\circ$ bin, so we caution against overinterpretation of results based only on this data point. The transitions are noted on the plots. Note the CO 7-6 transition plot also contains the C I $2p^2 :^3P_2 - ^3P_1$ transition at $370.4 \mu\text{m}$.

Figure 4: Plots are prepared as in figure 3 but the vertical scales are different. (a) The detected (see text) para- H_2O $1_{11} - 0_{00}$ ground state transition at $269.3 \mu\text{m}$. (b) The undetected ortho- H_2O $1_{10} - 1_{01}$ ground state transition at $538.3 \mu\text{m}$. (c) The ratio of the para- H_2O $1_{11} - 0_{00}$ to the continuum showing the fractional absorption (dimensionless scale). (d) The total IR emission ($\lambda > 105 \mu\text{m}$), the scale is $\mu\text{W m}^{-2} \text{sr}^{-1}$. (e) The undetected O_2 $3_2 - 1_2$ at $705.8 \mu\text{m}$. (f) The detected O I $2p^4 :^3P_0 - ^3P_1$ transition at $145.5 \mu\text{m}$. (g) The undetected Si I $3p^2 :^3P_1 - ^3P_0$ transition at $129.7 \mu\text{m}$. (h) The detected CH transition at $115.8 \mu\text{m}$.

Figure 5: (a) The C II $2p:2P_{3/2} - 2P_{1/2}$ fine structure ground state transition at $157.7 \mu\text{m}$. (b) The C I $2p^2 :^3P_1 - ^3P_0$ transition at $609.1 \mu\text{m}$. (c) The C I $2p^2 :^3P_2 - ^3P_1$ transition at $370.4 \mu\text{m}$. This is residual after subtracting an estimate of the CO 7-6 emission. (d)The ratio of C II to total far infrared continuum emission at wavelengths longer than $105 \mu\text{m}$ (dimensionless scale). (e) The N II $2p^2 :^3P_1 - ^3P_0$ fine structure ground state transition at $205.3 \mu\text{m}$. (f) The N II $2p^2 :^3P_2 - ^3P_1$ transition at $121.9 \mu\text{m}$. (g) The ratio of N II $122 \mu\text{m}$ to N II $205 \mu\text{m}$ emission for the central Galactic region (dimensionless scale). Farther from the Galactic center the ratio is dominated by noise. (h) The N II $205 \mu\text{m}$ to C II $157 \mu\text{m}$ ratio (dimensionless scale). The dotted and dashed lines are predictions from simple models

(see text).

COBE FIRAS 158 μm C⁺ Line Intensity



COBE FIRAS 205 μm N⁺ Line Intensity

